Chemistry–A European Journal
Research Article
doi.org/10.1002/chem.202401165
Chemistry Europe
European Chemical Societies Publishing
www.chemeurj.org

Rationalization of a Streptavidin Based Enantioselective Artificial Suzukiase: An Integrative Computational Approach

Laura Tiessler-Sala[+],[a] Jean-Didier Maréchal[+],*[a] and Agustí Lledós[+]*[a]

Dedicated to Professor Miquel Solà on his 60th birthday

An Artificial Metalloenzyme (ArM) built employing the streptavidin-biotin technology has been used for the enantioselective synthesis of binaphthyls by means of asymmetric Suzuki-Miyaura cross-coupling reactions. Despite its success, it remains a challenge to understand how the length of the biotin cofactors or the introduction of mutations to streptavidin leads the preferential synthesis of one atropisomer over the other. In this study, we apply an integrated computational modeling approach, including DFT calculations, protein-ligand dockings and molecular dynamics to rationalize the impact of mutations and length of the biotion cofactor on the enantioselectivities of the biaryl product. The results unravel that the enantiomeric differences found experimentally can be rationalized by the disposition of the first intermediate, coming from the oxidative addition step, and the entrance of the second substrate. The work also showcases the difficulties facing to control the enantioselection when engineering ArM to catalyze enantioselective Suzuki-Miyaura couplings and how the combination of DFT calculations, molecular dockings and MD simulations can be used to rationalize artificial metalloenzymes.

Introduction

Carbon-carbon bond formation reactions are essential for the synthesis of natural products, pharmacological active compounds and agrochemicals.[1,2] Among these are Suzuki-Miyaura cross-coupling (SMC) reactions,[3] one of the most powerful reactions for the formation of C–C bonds that has been widely used for constructing C(sp^2)–C(sp^2) bonds. The SMC reactions are catalyzed by palladium complexes and consist in the carbon-carbon formation between an aryl halide (organic electrophile) and an organoboron compound (organic nucleophile) in the presence of a base. The main advantage of this type of reactions is that they lead C–C coupled products in very high yields, all while operating under mild conditions.[4]

From extensive experimental and computational work,[5,6] a clear mechanistic picture of this reaction has emerged. The general mechanism of SMC reactions follows a catalytic cycle composed of three steps, as depicted in Figure 1. In the first step, the oxidative addition (OA), the organic halide is added to Pd(0), oxidizing it to Pd(II) and forming the organopalladium intermediate, with Pd bound to both the halide and the organic group. The transmetalation (TM) step is the most characteristic step of the reaction, in which the organic group bound to the boron species is exchanged for the halide in the coordination sphere at the palladium. In this way, the second organic group is transferred to the Pd complex. The last step entails the coupling between the two organic groups and the reduction of the metal to Pd(0), that why it is known as reductive elimination (RE).

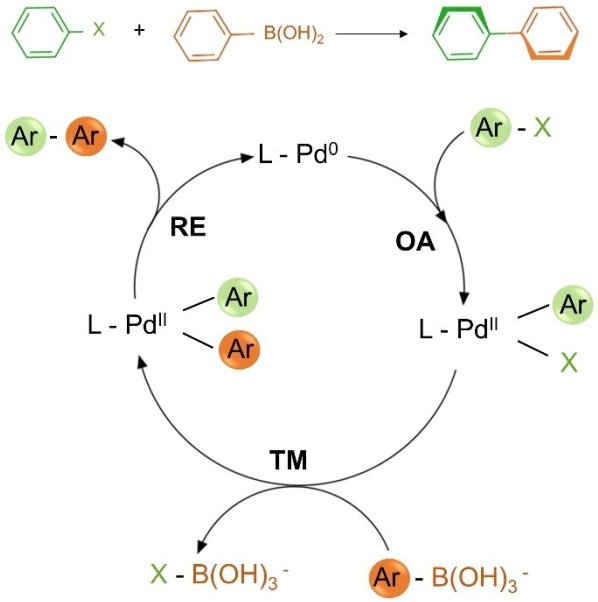

Figure 1. Catalytic cycle of a Suzuki-Miyaura reaction.

[a] L. Tiessler-Sala,[+] J.-D. Maréchal,[+] A. Lledós[+]
Departament de Química, Universitat Autònoma de Barcelona, Cerdanyola del Vallès, 08193 Barcelona, Spain
E-mail: jeandidier.marechal@gmail.com
agusti.lledos@uab.cat
[+] These authors contributed equally

Supporting information for this article is available on the WWW under https://doi.org/10.1002/chem.202401165

Despite the success achieved with Suzuki-Miyaura coupling reactions, the corresponding enantioselective versions are still challenging.[7] SMC are commonly used for the synthesis of biaryls, which are defined as two aromatic rings joined through a single C–C bond. However, biaryl products possess the characteristic of exhibiting axial chirality in the single C–C bond due to the hindered rotation of this bond. The electronic or steric effects from the different substituents generate a significant rotational barrier around the formed C–C σ bond, which enables the isolation of two distinct conformers. These are a particular case of enantiomers that receive the name of atropisomers, as represented in Scheme 1.[8]

Synthetic[9] and computational[10] efforts have been devoted to set in asymmetric Suzuki-Miyaura cross-coupling reactions for the enantioselective synthesis of biaryl atropisomers.[7,11] The approaches were based on the design of chiral ligands to facilitate catalytic enantioselective biaryl coupling.[12] Ascertain the origin of the enantioselectivity in these reactions has been matter of debate. It was thought that the enantioselectivity is dictated by the conformation of the intermediate just prior to the reductive elimination step. However, a thorough computational study of SMC for the synthesis of tetra-ortho-substituted biaryls revealed that the enantioselectivity is influenced by all the three steps in the catalytic cycle.[13]

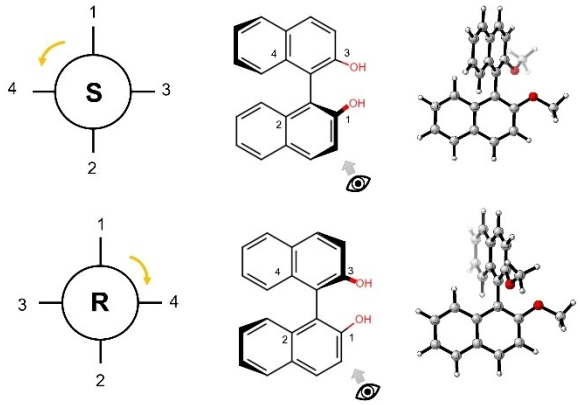

Scheme 1. Concept of atropisomers for biaryls.

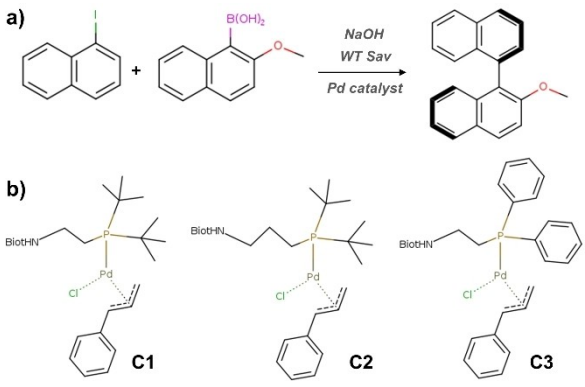

Scheme 2. a) Synthesis of 2-methoxy-1,1′-binaphthyl by SMC. b) Biotinylated cofactors experimentally tested.

An alternative approach for asymmetric SMC catalysis is to leverage second coordination sphere effects, and this can be done by means of biocatalysis.[14] In particular, artificial metalloenzymes (ArMs),[15] built up by combining a non-native catalytically active transition metal cofactor within a protein scaffold, are promising entities to provide a well-defined second coordination sphere for asymmetric catalysis. In this direction, Ward designed an ArM, based on the streptavidin (Sav)-biotin technology,[16] that is able to catalyze the synthesis of chiral biaryls by the SMC (in their worlds, an artificial Suzukiase).[17] The design of the ArM consisted in anchoring a modified biotin cofactor with palladium into Sav or avidin scaffold. Specifically, the biotin cofactor is connected with a phosphine ligand of palladium by means of a linker. Five different biotinylated Pd-cofactors were synthesized and evaluated with either Sav or avidin for the synthesis of a biaryl compound, 2-methoxy-1,1′-binaphthyl (Scheme 2a).

Screening results suggested that most promising combination was wild type (wt)-Sav with catalyst **C1**, **C2** or **C3** (Scheme 2b). Previous studies on biotin-Sav ArM suggested that position S112 and K121 could be mutated to optimize the reaction due to its proximity to the active site. Accordingly, the three different biotinylated catalysts were screened against a library of Sav with mutations on S112 and K121. Results of this screening show that higher conversions are obtained for *t*-Bu catalysts (**C1** and **C2**) than Ph catalyst (**C3**). Focusing only on cofactors **C1** and **C2**, an important feature was elucidated: variation of the length of the linker yields different enantiomeric products.

Mutated systems S112M and K121 A with longer biotin-phosphine linker (**C2**) are the ones that afford the highest enantiomeric excess (ee) for *S* enantiomer, whereas system K121E with shorter linker (**C1**) affords the highest ee for *R* enantiomer. For this reason, mutation K121E was identified as a good candidate for the screening of double mutants with cofactor **C1**. The results indicate that double mutant S112Y-K121E yields the highest ee (%) and TON for *R* enantiomer, which was improved up to 90% ee by varying the experimental conditions (Table 1). This double mutant was crystallized, and the disposition of the metallic cofactor and the mutations can be observed in Figure 2.[17]

In the experimental study they were able to afford an enantioselective artificial Suzukiase for the synthesis of binaphthyls. However, it remains extremely challenging to rationalize or predict how the mutations and the length of the different cofactors lead the preferential synthesis of one atropisomer over the other. The main objective of this work is to try to explain rationally and qualitatively how different

Table 1. Enantiomeric excess obtained depending on Sav system and cofactor.[17]

	Protein				
	WT	K121E	K121A	S112M	S112Y-K121E
C1	58 (*R*)	76 (*R*)		14 (*S*)	90 (*R*)
C2	10 (*S*)		47 (*S*)	44 (*S*)	

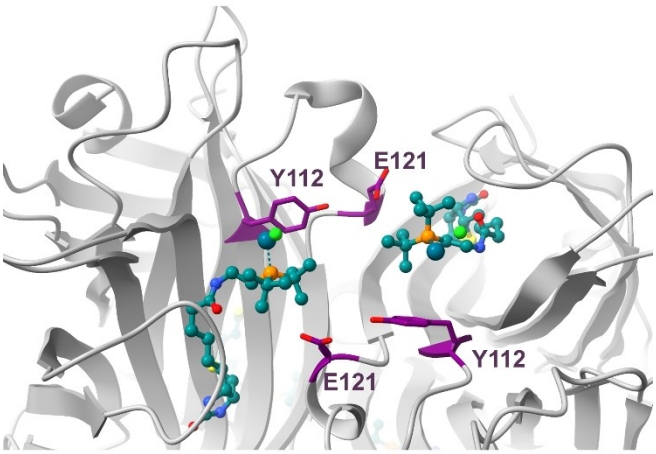

Figure 2. Binding pocket of X-ray structure of double mutant S112Y-K121E (PDB = 5cse).

enantioselectivities are obtained using an integrative computational approach[18] that we have already employed to unravel the features of other ArMs.[19] Figure 3 schematizes the protocol employed in the simulations, that will be described with more detail in the Methodology section. Since it is not feasible to study all mutated systems, this work focused on the three Sav systems with different behaviors: WT, S112M and S112Y-K121E.

Methodology

The general workflow was composed of four steps (Figure 3): 1) Characterization of the full reaction mechanism and identification of key intermediates and transition states (TSs) in water solvent using Density Functional Theory (DFT) calculations; 2) Modeling of each Sav mutated system with precatalytic cofactors **C1** or **C2** bound, introduced previously by dockings using as input the PDB structure 5CSE,[17] and refined by Molecular Dynamics (MD) simulations to assess the stability of each system and the flexibility of each cofactor; 3) Insertion of **OA** intermediate structures into the proteins by protein-ligand approaches; **4)** Conducting MD simulations to evaluate the overall interaction between the protein and the intermediates (**OA**) or TS (**RE-TS**) leading to the different stereospecific products.[18]

DFT calculations: A mechanistic DFT study of the full catalytic cycle of the Suzuki-Miyaura reaction was performed in water solvent with biotinylated cofactor **C1** using as substrates 1-iodonaphthalene and 2-methoxy-1-naphthaleneboronic acid. Each intermediate and TS of the reaction step was characterized by vibrational frequency analysis, and the Gibbs barriers were calculated to establish the rate determining step of the reaction. Different TSs leading to either the *R* or the *S* atropisomers were also characterized. All geometry and frequency DFT calculations were performed with the Gaussian16[20] programs using B3LYP[21] functional including Grimme's dispersion D3 (B3LYP–D3).[22]

Optimizations were carried out in water solvent (SMD continuum model)[23] with ε = 78.35 with basis set 1 (BS1). In BS1 Pd atom is described by means of an SDD effective core potential (ECP) for the inner electrons and its associated double-ζ basis set for the outer ones,[24] complemented with a set of *f*-polarization functions,[25] and the basis set 6–31G(d,p)[26] is used for non-metallic atoms. Energies in water were refined by means of single-point calculations at the optimized BS1 geometries using an extended basis set (BS2). BS2 consists of the def2-TZVP basis set for the main-group atoms, and the quadruple-ζ def2-QZVP basis set for Pd, together with the def2 ECP.[27] An additional correction of 1.9 kcal/mol was applied to the Gibbs energies to change the standard state from the gas phase (1 atm) to the condensed phase (1 M) at 298.15 K

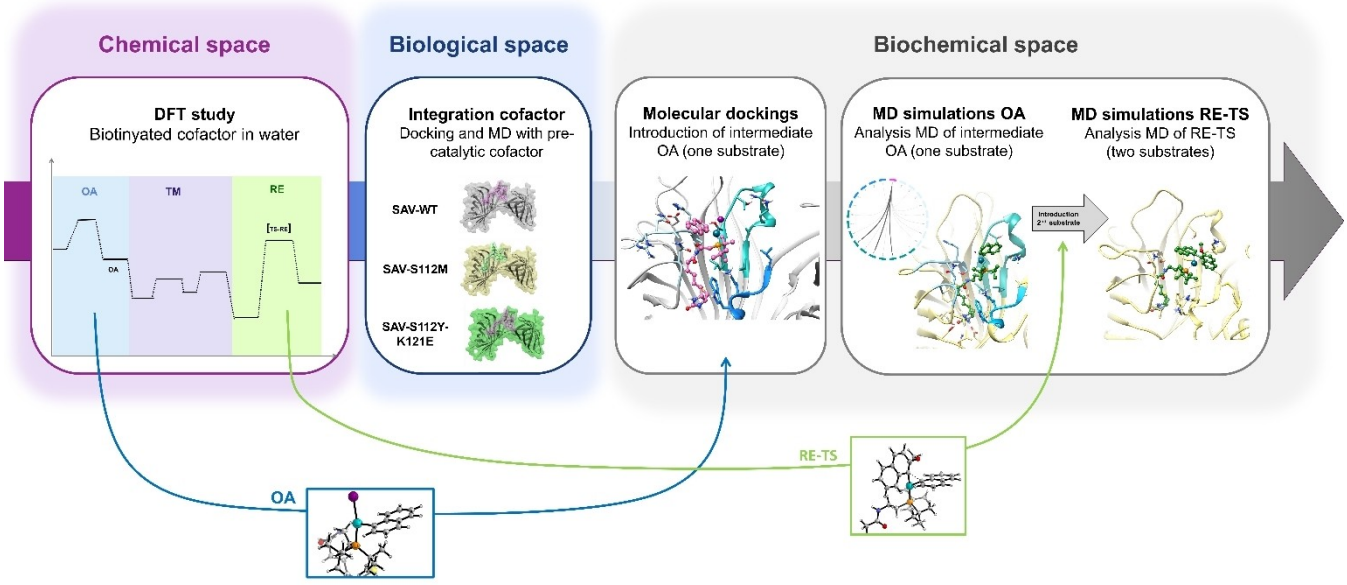

Figure 3. Steps followed during molecular modeling workflow.

(ΔG1 atm→1 M). In this way, all the energy values in the energy profiles are Gibbs energies in water solvent calculated using the formula:

$$G = E(BS2) + G(BS1) - E(BS1) + \Delta G^{1atm \rightarrow 1M}$$

Molecular dockings: Docking calculations were performed to introduce the optimized biotinylated precatalytic cofactors **C1** or **C2** bound in wt and Sav mutated systems, using as initial input the X-ray structure of the artificial Suzukiase C1·S112Y-K121E (pdb code: 5CSE).[17] Protein-ligand docking approaches allowed to incorporate QM-optimized reaction intermediates or TSs structures (both pro-*R* and pro-*S* structures) into the binding site of the different protein systems. Docking calculations were performed with GOLD5.8[28] with an evaluation sphere of 15 Å and considering side-chain flexibility in key residues and the ligand (except the biotin bicyclic moiety). Genetic algorithm parameters were set to 50 GA runs, a minimum of 100.000 operations and the rest of the parameters were left to default. Due to the complexity of Suzuki-Miyaura reaction and the great variance of docking solutions it was not possible to draw any conclusion. Instead the protocol that was followed consisted on performing docking calculations and MD simulations with the first intermediate of the reaction (**OA**), which only contains one of the substrates. The intention was to study the behavior of the intermediate OA containing only the first substrate in both pro-*R* and pro-*S* conformation and then elucidate if the entrance of the second substrate would be feasible.

Molecular dynamics simulations: The best docking results were employed as starting points for the MD simulations which allowed to assess the stability of each system and the flexibility of each cofactor. All MD simulations were prepared with the xleap from Amber20.[29] Each system was solvated using an explicit solvent approach by embedding it into a cubic box with a neutral charge (neutralization with Na^+ and Cl^-). The AMBER19SB[30] force field was used for proteins, GAFF[31] for non-standard residues, ions94.lif for ions and TIP3P[32] for water. The parameters to characterize palladium containing structures were calculated using MCPB.py.[33] Charges were calculated using RESP[34] (Restrained ElectroStatic Potential) model and force constants and equilibrium parameters between metal and residues were obtained through the Seminario method.[35] Basis sets and parameters employed for these DFT calculations were the same as specified previously in the DFT calculations section.

The AMBER program was used to perform the MD simulations following a standard simulation protocol. The Langevin integrator[36] was used with a time step of 1 fs with periodic box conditions. The simulation was performed at constant temperature and pressure by using a barostat coupled to a bath of 1.01325 bar. A cut-off of 1 nm was used for non-bonded interactions (short-range electrostatic and van der Waals interactions) and the PME[37] method was applied for long-range electrostatic interactions. Additionally, SHAKE[38] algorithm was used to constrain bonds that involve hydrogen and the rigid model was used to represent the water molecules. To avoid steric clashes and relax the system energy minimizations were performed, followed by several equilibration steps to heat the system from 100 K to 300 K in order to allow thermalization of water and side-chains. Finally, production runs of 200–300 ns were carried out. Clustering of intermediates **OA** was performed using cpptraj[29] and the interactions between the intermediates and Sav were monitored during MD simulations using getContacts.py script. To assess the possibility of the entrance of the second substrate, an analysis of all the possible clashes between the second substrate and surrounding residues was performed using Chimera UCSF.[39] This study allowed to discern if there are favored conformations for the entry of the second substrate. Finally, MD simulations of the **RE-TS** with the two substrates were performed.

Results and Discussion

Studying the Reaction in Water with DFT

Our computational protocol starts by computing with DFT calculations a complete energy profile of the reaction in solution (water solvent), with location of intermediates and transition states, using a minimal model of the reactive system. These models are usually called theozymes.[40] Indeed, there are some reports of asymmetric SMC catalysis in water,[41] and the cofactor alone is able to catalyze the reaction, although with lower conversions than with the protein and yielding a racemic mixture.[17]

The complete Suzuki-Miyaura reaction was calculated in water with DFT using the full biotinylated cofactor **C1** as a catalyst and iodonaphtalene and 2-methoxy-1-naphtaleneboronic acid as a substrate. Optimized structures of **C1** and **C2** biotinylated cofactor employed in DFT calculations are displayed in Figure S1. The Gibbs energy profile that leads to the *R* atropisomer with lower barrier is represented in Figure 4. An overall scheme of the reaction mechanism, together with 3-D structures of all the optimized species along the catalytic cycle are collected in the *Supporting Information* (Scheme S1 and Figure S2). Over this section, we will discuss in more detail the results of each of the three steps of the reaction and provide more insights with supplementary calculations that have been conducted for each step.

It has been established that, under catalytic conditions, oxidative addition of aryl halides occurs to a 12-electron monoligated palladium complex and the transmetalation step proceeds via a tetracoordinate boronate intermediate with a Pd–O–B linkage.[5] Both assumptions have been taken into account in the computational study.

In a Suzuki-Miyaura reaction the first step is the Oxidative Addition (OA). This first stage comprises the formation of the adduct between the aryl halide (1-iodonaphtalene in this case) and the biotinylated palladium catalyst **C1** (Pd(PR(*t*-Bu)$_2$; R = biotinylated chain with a (–(CH$_2$)$_2$–) linker). This step leads to the **OA** intermediate, which contains a T-shaped tricoordinated palladium center. The addition of the 1-iodonaphatlene can take place via two different pathways depending on whether the iodine (pathway A) or the aryl (pathway B) is positioned in a *trans* disposition relative to the phosphine (see *Supporting*

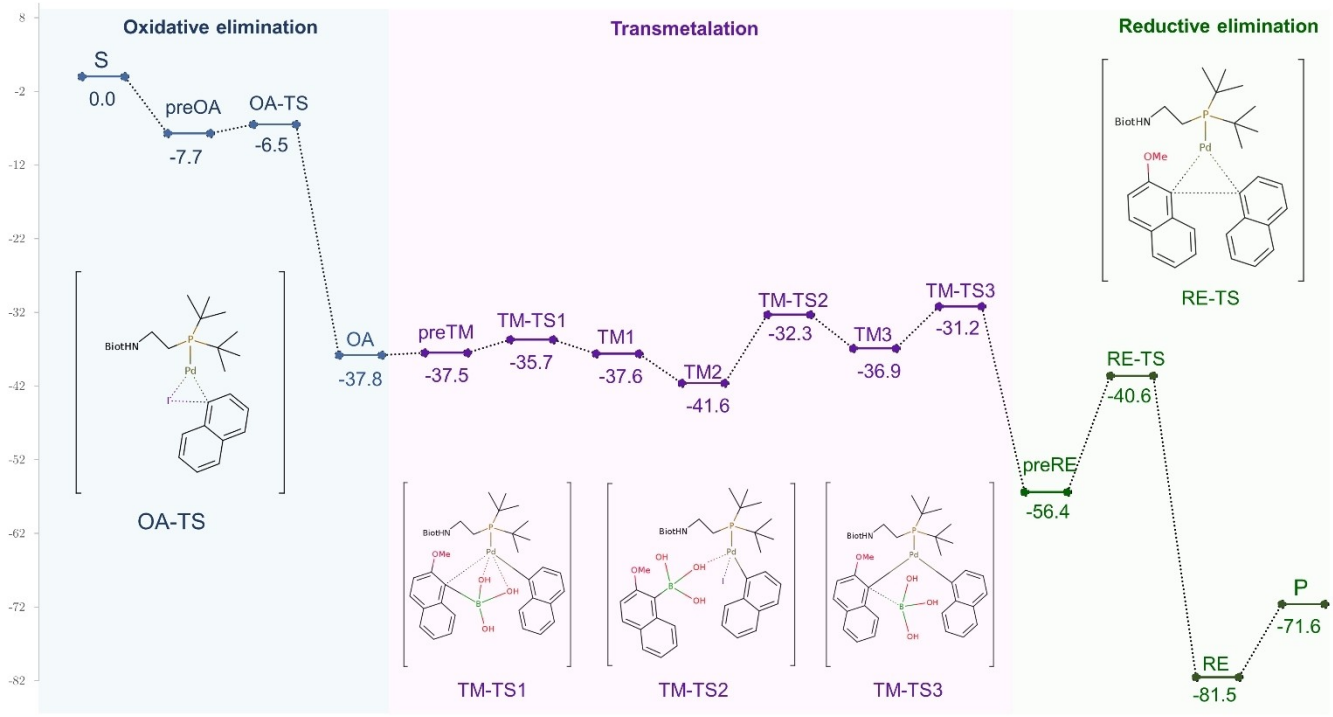

Figure 4. Gibbs energy profile in water obtained with cofactor C1. Gibbs energies in kcal mol^{-1}.

Information, Scheme S2 and Figure S3). Both pathways A and B exhibit nearly identical Gibbs energy barrier, measuring 1.2 kcal/mol and 1.3 kcal/mol, respectively. However, when looking at the products of the two oxidative addition pathways, **OA_B** is found to be 12.4 kcal mol^{-1} higher than **OA_A**. In **OA_A** the iodine is *trans* to the phosphine and the aryl is pointing toward the vacant position, while in **OA_B** the aryl is *trans* to the phosphine. The high *trans* influence of the aryl destabilizes the **OA_B**, as it shows the Pd–P distance (2.32 Å in **OA_A** and 2.43 Å in **OA_B**). Therefore, due to the higher stability of **OA_A**, for the rest of the reaction it was decided to consider the product of pathway A for the sake of simplicity. The results for this first step are in concordance with DFT study of Patel *et al.*, in which they calculated the Gibbs energy profile for the SMC of tetra-*ortho*-substituted biaryls using different ligands.[13] Their barrier for pathway A is 0.7 kcal/mol, the 0.5 kcal/mol difference with our study could be attributed to the use of different ligands or substrates.

In addition, the formation of **OA_A** can occur via two pathways depending on the orientation of the naphthyl group. The difference between the two possible OA products (**OA_A1** vs **OA_A2**) is 0.4 kcal/mol (Figure 5a). Since none of the products exhibit any unfavorable contacts, the energy gap between them is small, suggesting that both products are equally feasible in terms of energy. To assess the energetic cost of the transition between both conformations, the rotation around Pd–C_{aryl} bond was analyzed. Results of this rotation scan, depicted at Figure 5b, reveal that the rotation of this bond has a barrier of 19.0 kcal/mol. Despite the minimal energetic difference between **OA_A1** and **OA_A2**, the transition between the two products is hindered by a barrier that is too high for reaction conditions. Therefore, it is assumed that once one conformation is adopted, there will be no transition towards the other conformation. This differentiation sets up the first layer for the enantioselectivity of the reaction. For simplicity, DFT calculations for the rest of the reaction in the energy profile of Figure 4 were performed for **OA_A1**, which is slightly more

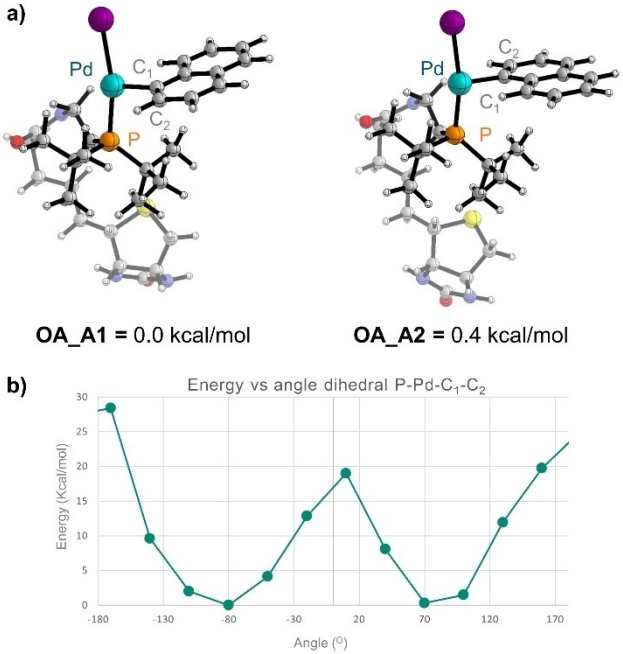

Figure 5. a) Intermediates formed in the oxidative addition step. b) Torsion scan between intermediates OA_A1 and OA_A2.

stable, and it is assumed that values for the other pathway will be similar. We will discuss later on the consequences of this conformational issue in **OA** intermediates on the enantioselectivity.

In the transmetalation (TM) step, the second organic substrate, containing a boronate group, is introduced and initially coordinates to the Pd through one hydroxyl. In a three-step process, the iodine and the boric acid are removed sequentially, while the bond between the entering substrate (2-methoxy-naphthalene) and the Pd is formed. Overall, the TM step involves three TSs, each characterized by Gibbs energy barriers of 1.8, 8.8 and 5.7 kcal/mol, respectively (see a detailed scheme of the transmetalation mechanism in Scheme S3, *Supporting Information*). The product of the TM has both organic substrates bound to the Pd catalyst (**preRE**). It is important to note that in this step the entrance of the second substrate can occur in two different orientations. In the *close* conformation (**c**) the two non-metalated rings of the naphthalene ligands are in the same side of the plane defined by the phosphine, palladium and metalated carbon of the methoxy-naphthalene, while in the *far* (**f**) conformation they are in opposite sites. Both conformations in the **preRE** step are represented in Figure 6. However, for simplicity, only the far conformation was considered in the energy profile of Figure 4. The stability of each conformation will be studied at the last step of the reaction (**RE**), in which the C–C bond between the two substrates is formed, yielding the biaryl product. The Gibbs energy barrier of this step is 15.8 kcal/mol, making it the highest barrier of the full reaction and therefore the rate-determining step. However, the computed energy profile (Figure 4) shows that in our system oxidative addition and transmetalation steps are irreversible, preventing the equilibration of all the intermediates formed before the reductive elimination step. As pointed out in the Patel study,[13] this result implies that all the three steps in the catalytic cycle contribute to the overall enantioselection.

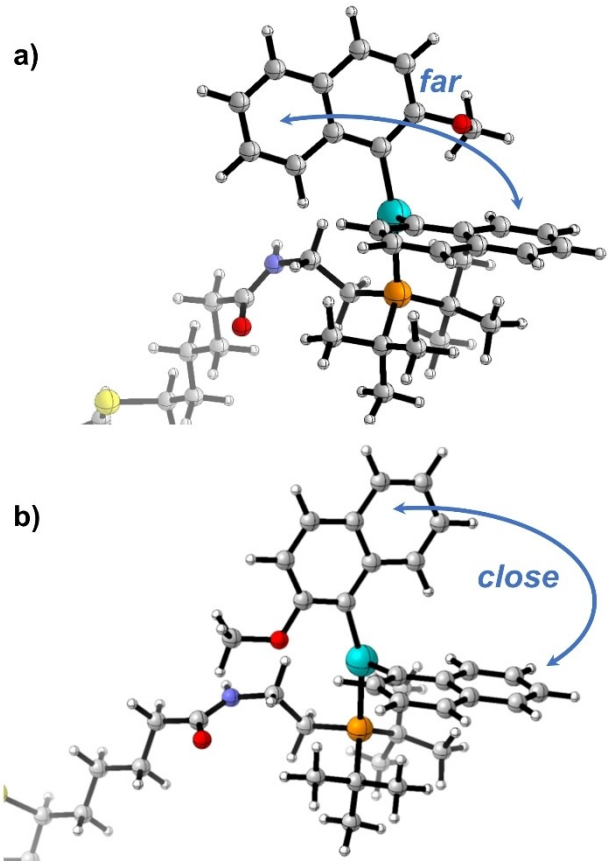

Figure 6. Representation of *far* and *close* conformations in preRE intermediate.

As discussed before (Figure 5), after the OA step there are two possible orientations for the coordinated naphthyl (**OA_A1** and **OA2_2**) that cannot interconvert. The transmetalation step introduces the methoxy-naphthyl in the palladium coordination sphere, either in a *far* or *close* conformation with respect the first naphthyl, giving rise to four possible **RE-TS**s. We have computed the four RE transition states (see Figure S4, *Supporting Information*). The Gibbs energy profile in Figure 4 incorporates the lowest transition state, that involves **OA_A1**/*far* conformation and yields the *R* atropisomer. The next one in energy ordering (1.4 kcal/mol above) is **OA_A2**/*far* and yields the *S* atropisomer. For both **OA_A1** and **OA2_2** orientations of the naphthyl, the *close* RE transition states are less stable than the *far*. We hypothesize that this difference (**OA_A1**/*close*: 4.3; **OA_A2**/*close*: 5.9 kcal/mol above **OA_A1**/*far*) is caused by the steric hindrance between the naphthyl rings in the *close* conformation. Calculations performed with **C2** catalytic cofactor give the same ordering (the corresponding values are 0.0, 0.9, 3.4 and 3.7 kcal/mol, Figure S5, *Supporting Information*). Considering only the *far* conformations, from the RE relative Gibbs energy barriers commented before it can be established that intermediate **OA_A1** leads preferentially to the *R* atropisomer (pro-*R*), whereas the form **OA_A2** leads preferentially to the *S* atropisomer (pro-*S*). For the cofactor **C1** in water the energy difference between the lowest pro-*R* and pro-*S* TSs is only 1.4 kcal/mol. In the next sections we will analyze how this picture is affected by the protein.

Molecular Modeling of the Protein Systems

Docking and MD Simulations with Precatalytic Cofactors

Molecular docking simulations are conducted to introduce both precatalytic cofactors, **C1** (short, –$(CH_2)_2$–) and **C2** (long, (–$CH_2)_3$–), into the three different Sav systems (WT, S112M and S112Y-K121E). These precatalytic cofactors contain the biotinylated Pd catalyst saturated with chloride and a cinnamyl moiety (see Figure S1, *Supporting Information*). Docking solutions reveal flexibility in the position of the cinnamyl and chloride moieties, attributed to the rotation of the bonds in the linker region, which is more pronounced when linker is longer in the **C2** cofactor. Consequently, MD simulations are performed using as input the best docking solutions, which were selected according to scoring function and similarity to crystal structure. The aim of the MD simulations is to explore the conformational space of the protein and to assess the behavior of the two

catalytic cofactors before the Suzuki-Miyaura reaction. Significant differences are observed among distinct Sav systems and cofactors. Considering the protein structure, it does not suffer significant changes across the MD simulations, except some mobility in the flanking loops between the β-barrels, which could be relevant for the catalysis. The biotin part of precatalytic cofactor is mainly fixed due to the presence of several hydrogen bond interactions with Sav residues. Contrarily, the linker part of the cofactor and the cinnamyl moiety display a remarkable flexibility by exploring the available conformational space extensively. This observation is supported by the X-ray structure of Sav-S112Y-K121E with the precatalytic cofactor,[17] the full structure is resolved except for the cinnamyl region, which density is not determined probably due to its high flexibility.

From these simulations it can be determined that the cofactors in the resting state of the reaction can acquire two very different conformations, which will be referenced from now on as: *biotin-up* and *biotin-down* (Figure 7). In the b*iotin-up* conformation, the P(*t*-Bu)$_2$ of the biotinylated cofactor is in the upper region of the binding site with the chloride and cinnamyl moiety facing down towards the inside of the active site. Contrarily, in the *biotin-down* disposition the P(*t*-Bu)$_2$ of the biotinylated cofactor is in the lower site of the binding site, under the Pd atom, and the chloride and cinnamyl moiety, which are facing the solvent. Depending on the system or the length of the cofactors the tendency to be on the *biotin-up* or the *biotin-down* disposition changes. A dihedral angle between the catalyst (atoms Pd and P) and Sav (α-carbon from residues 99 and 100) is monitored during MD to assess the biotin conformation *(*Figure S6, *Supporting Information*).

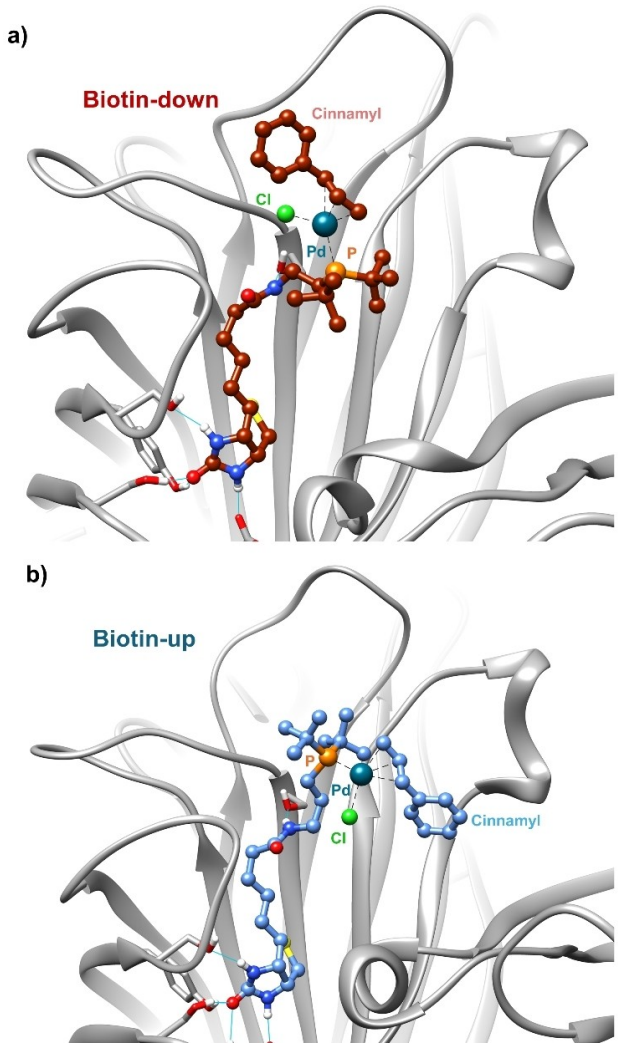

Figure 7. Conformations of precatalytic cofactor **C1** from MD simulations: a) *biotin-down*, b) *biotin-up.*

MD simulations with the **C1** precatalytic cofactor display a tendency for the *biotin-down* conformation, with the cinnamyl and the chloride moieties facing the solvent. The short length of the linker seems to favor the *biotin-down* conformation, without the possibility of rotating towards the *biotin-up* conformation. However, differences are observed between the three systems related to the interactions of the cofactor and close-by mutated residues (Figure S7 and Table S3*, Supporting Information*). In the Sav-WT system, the *biotin-down* conformation is maintained during all MD simulations and the cinnamyl moiety swings between the two sides of Sav. It either interacts with loop containing Asn49 and His87 or Lys121 on the opposite site. In Sav-S112M, the main disposition of cofactor **C1** during the MD is also *biotin-down*. However, at some points the biotinylated cofactor can rotate and acquire the *biotin-up* conformation. The capability to acquire the up conformation may be related to the mutation that has been introduced, close-by residue Ser112 has been mutated to Met, a much longer and hydrophobic residue. Contacts during MD simulations between the precatalytic cofactor **C1** are higher with Met than in Sav-WT with Ser. Met112 mainly interacts with the P(*t*-Bu)2 from the cofactor and interacts less with cinnamyl. The rest of interactions of the cofactor and the swinging movement between regions is also observed in this system.

In the case of Sav-S112Y-K121E, only the *biotin-down* conformation is observed in the MD simulations, there is no rotation of the biotin toward the *biotin-up* conformation at any moment. The mutation of Ser112 to aromatic Tyr increases considerably the interaction with the cinnamyl, maintaining the precatalytic cofactor in the center of the biotin pocket. Mutation Lys121 to Glu leads to a decrease of the interaction with cinnamyl moiety, which also causes cinnamyl to remain in the center of the binding site. From this analysis it can be concluded that both mutations favor the *biotin-down* conformation.

MD simulations with the longer precatalytic cofactor **C2** tend to acquire the *biotin-up* conformation, the cofactor can switch from the *biotin-down* to the *biotin-up*. The additional carbon atom before the P(*t*-Bu)$_2$ group provides an increased capacity for the cofactor to rotate. However, there are some differences between Sav-WT and Sav-S112M due to the mutation introduced. In Sav-WT, the prevalent conformation is *biotin-up*, but in different monomers of Sav the transition from *biotin-up* to *biotin-down* and vice-versa can be observed, indicating that both conformations are inter-convertible. Contrarily, in Sav-S112M, when the *biotin-up* conformation is

acquired, it remains in this disposition and makes no transition to *biotin-down*. Once the cofactor has rotated toward the *biotin-up* conformation, Met112 remains under the cofactor interacting with cinnamyl hindering the transition to *biotin-down*. Interaction analysis values indicates that generally Met112 interacts more with the cofactor, especially with the cinnamyl compared to the WT (Figure S8 and Table S4, *Supporting Information*). In both systems, when in the *biotin-up* disposition, the cinnamyl interacts with a hydrophobic patch found in the interface of the dimer containing Lys121, Val123 and Leu124 from both monomers.

This initial MD study reveals that the precatalytic cofactors can acquire two different dispositions that depend both on the length of the cofactor and the mutations introduced in the system. It can be concluded that the relevance of this study relies on the fact that the different dispositions of the cofactor can affect the entrance of the two substrates.

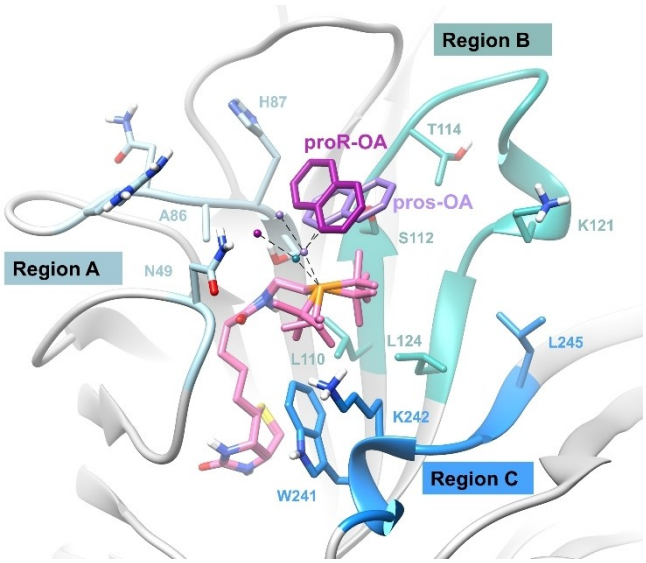

Figure 8. Sav biotin-binding pocket and WT–C1 docking results for pro-*S* and pro-*R* OA intermediates.

Docking of OA Intermediates

The DFT study determined that the oxidative addition intermediate, only involving the first substrate of the SMC reaction, can have two conformations, **OA_A1** or **OA_A2** (Figure 5). As discussed before, each of these OA intermediates will lead to a *far* conformation (more stable than *close*) of **RE-TS** when the two substrates are present, *far*-pro-*R* and *far*-pro-*S* depending if they come from pathway **OA_A1** or **OA_A2**. Therefore, the location of the first substrate affects the binding of the second one and the OA intermediate is the first layer of enantioselectivity. First, molecular docking of the two possible OA intermediates, pro-*R*-OA (**OA_A1**) and pro-*S*-OA (**OA_A2**) will be performed, followed by MD simulations. The localization of the intermediate OA (with only the first naphthalene substrate) will allow to later superpose **RE-TS** and study if the entrance of the second substrate would be possible. Instead of performing calculations for all five selected cases, simulations are performed for WT-**C1**, S112M-**C2** and S112Y-121E-**C1**, as they have higher ee differences (Table 1).

Docking calculations are performed for both pro-*R*-OA and pro-*S*-OA for all Sav systems using as input the most populated cluster of MD simulations with the precatalytic cofactor (Table S6, *Supporting information*). The conformation of the precatalytic cofactor is maintained fixed and the naphthyl substrate and the iodine are docked, allowing rotation. In all cases, WT-**C1**, S112M-**C2** and S112Y-K121E-**C1**, no relevant differences are found between pro-*R* and pro-*S* docking results, the scorings values and the disposition of the substrates are very similar. This means that the probability of the first substrate to acquire pro-*R* or pro-*S* conformation is the same at this stage of the reaction. Results of WT-**C1** are represented in Figure 8 as an example. The biotin pocket has been divided in three regions that will be referred from now on as region A, B and C. Region A includes residues Ala86 and polar residues Asn49 or His87, region B includes mutant residue Ser112 and Lys121 and hydrophobic residues Leu110,124. Region C in the other monomer includes Trp241, Leu245, and mutant Lys242. In the three cases, the substrate is found interacting with region A of Sav, mainly with residue 112.

MD Simulations of OA Intermediates

MD simulations, initiated from the docking positions, are performed for the three Sav systems with pro-*R* and pro-*S* OA intermediates. Clustering of the intermediate OA is performed using cpptraj to find the most common conformation during the MD simulation (Figure S9, *Supporting information*). The prevalence of each cluster and the tendency of the pro-*R*-OA and pro-*S*-OA intermediates to acquire the *biotin-up* or *biotin-down* conformation are analyzed by cluster and summarized in Table 2. An additional study is conducted to see if the entrance of the second substrate would be feasible by looking at the possible clashes that would happen between the second substrate and the protein if it were to bind. To achieve this, the **RE-TS** structure is superposed to the OA intermediate during the MD simulation to extrapolate the position of the second substrate and the clashes are monitored with Chimera UCSF. Mean value of clashes in each cluster are displayed in Table 2 and represented in Figure S9 of the *Supporting information*. To assess the *biotin-up* and *biotin-down* conformations of pro-*R*- and pro-*S* OA intermediates the dihedral angle between atoms P and Pd from OA intermediate and alpha-carbon from residues 99 and 100 is monitored during MD simulations (Figure S10 of the *Supporting information*).

Analysis from Table 2 yields two observations: 1) The pro-*R*-OA intermediate tends to acquire the *biotin-down* conformation preferably, whereas the pro-*S*-OA acquires the *biotin-up* disposition; 2) The entrance of the second substrate is more probable for the pro-*R*-OA in the *biotin-down* conformation and for the pro-*S*-OA in the *biotin-up* conformation. However, as we will explain in this section, these tendencies also depend on the

Table 2. Analysis of the results of MD simulations with pro-*S* and pro-*R* OA intermediates.

	proR				proS			
	% Cluster	Disposition	Region	Clashes	% Cluster	Disposition	Region	Clashes
Sav-S112M **C2**	41.8%	Down	B	**5.8**	87.2%	Up	B-C	**2.3**
	17.3%	Down	B		8.9%	Up	B-C	
	36%	Up	B-C	9.8				
Sav-WT **C1**	70%	Down	B	15.3	71.4%	Up	B-C	**12.5**
	28%	Down	A	**5.2**	23%	Down	A	16.8
Sav-S112Y-K121E **C1**	45%	Down	A	**11.3**	52.5%	Down	B	28.6
	35.8%	Down	B	15.4	27.4%	Down	A	
					15.9%	Up	B-C	**6.7**

mutations introduced on the system and the length of the cofactors. Now, we will comment a bit further these two aspects for each case and relate it to the experimental results.

In the case of S112M-**C2**, as seen in the MD simulations with the precatalytic cofactor, when the cofactor is longer the tendency to acquire *biotin-up* conformation increases probably due to the ability to rotate thanks to the extra carbon in the linker. Still, different behaviors are obtained for pro-*R*-OA and pro-*S*-OA systems. In the pro-*R*-OA, during 59.1% of the simulation the cofactor remains in the *biotin-down* conformation, interacting with Met112, Thr114 and Lys121 from region A (Figure 9b). However, the cofactor slightly rotates, and the substrate situates on top of Met112, acquiring the *biotin-up* conformation during the rest of simulation (36%). On the other hand, in the case of pro-*S*-OA, the cofactor almost immediately acquires the *biotin-up* conformation and it is maintained during all simulation. In the *biotin-down* conformation the substrate is interacting with region B–C, naphthyl is found between Met112 and Lys242 and surrounded by hydrophobic residues, Trp241, Leu110-124 and Lys121. The mutated Met112 changes its rotamer position slightly when acquiring the *biotin-up* conformation, which difficulties acquiring the *biotin-down* conformation again (Figure 9e).

The access of the second substrate is easier in the pro-*S* *biotin-up* conformation, with fewer clashes (2.3) with surrounding residues compared to the pro-*R*-OA (5.8-9.8), suggesting that more *S* product should be expected (Table 2). In the pro-*R*-OA, the entrance of the second substrate has less clashes in the *biotin-down* conformation and as the clashes are low in this conformation (5.8) for most of the simulation (59%), the *R* product should also be expected, but in lesser quantities than the S product. This is in qualitative concordance with the experimental results, 44% ee *S* (Table 1), indicating the predominant formation of the *S* atropisomer, though with a minor presence of the *R* atropoisomer.

The additional carbon of **C2** cofactor allows better rotation of the cofactors and Met112 mutation keeps the naphthyl substrate in the *biotin-up* form interacting with Lys121 and the hydrophobic patch between monomers. It can be hypothesized that both the long cofactor and mutation S112M favor the *biotin-up* conformation, consequently, the entrance of the second substrate and reactivity is much more probable in this pro-*S*-OA.

When using the cofactor with the short linker (**C1**) in WT-**C1** and S112Y-K121E-**C1**, similarities can be observed in the behavior of the pro-*R*-OA form, but difference in the pro-*S*-OA. In both systems, for pro-*R*-OA, the *biotin-down* conformation is observed all through the MD simulation and, depending on the cluster, the naphthyl substrate is either interacting with region A or with region B. For pro-*S*-OA, in the WT, the MD simulations pro-*S*-OA starts from the *biotin-down* conformation and remains in this disposition the first 23% of simulation, interacting with region A. However, it rotates and acquires the *biotin-up* conformation for remaining 71.4%, in which it is interacting with region B–C, mainly with Lys121, Leu110-124 and Ser112 (Figure 9a,d).

In S112Y-K121E, an opposite behavior is observed (Figure 9c,f). Pro-*S*-OA immediately acquires the *biotin-up* conformation, in which the naphthyl substrate is in the lower region of the binding site interacting with Trp241 and mutated Glu242 from region B–C. However, these interactions are not maintained as in the WT or S112M form, in which the naphthyl is interacting with Lys121 or Met112. Therefore, it rotates again and for the rest of the simulation the disposition is *biotin-down*, facing the solvent. In this *biotin-down* conformation there are two clusters. In the first cluster, the substrate is interacting with region B, while in the second cluster the substrate is interacting also with region A, mainly with Tyr112. Tyr112 is precisely one of the mutated residues, it is observed that this Tyr directly interacts with $(t\text{-}Bu)_2$ of cofactor. Probably, this interaction keeps the cofactor in the *biotin-down* conformation causing of the inability to rotate towards the *biotin-up* conformation. Therefore, mutations S112Y and K121E favor *the biotin-down* conformation.

Regarding the entrance of the second substrate for the WT, the pro-*S*-OA acquires the *biotin-up* conformation, but in this conformation there are more clashes (12.5) for the entrance of the second substrate than the pro-*R* in the *biotin-down* conformation, in which during 28% of the simulation there are 5.2 clashes. Therefore, in the WT the entrance of the second substrate is more probable in the pro-*R*-OA conformation, justifying the experimental 58% ee *R*. In the case of S112Y-K121E it can be observed that the entrance of the second

Research Article
doi.org/10.1002/chem.202401165
Chemistry Europe
European Chemical Societies Publishing

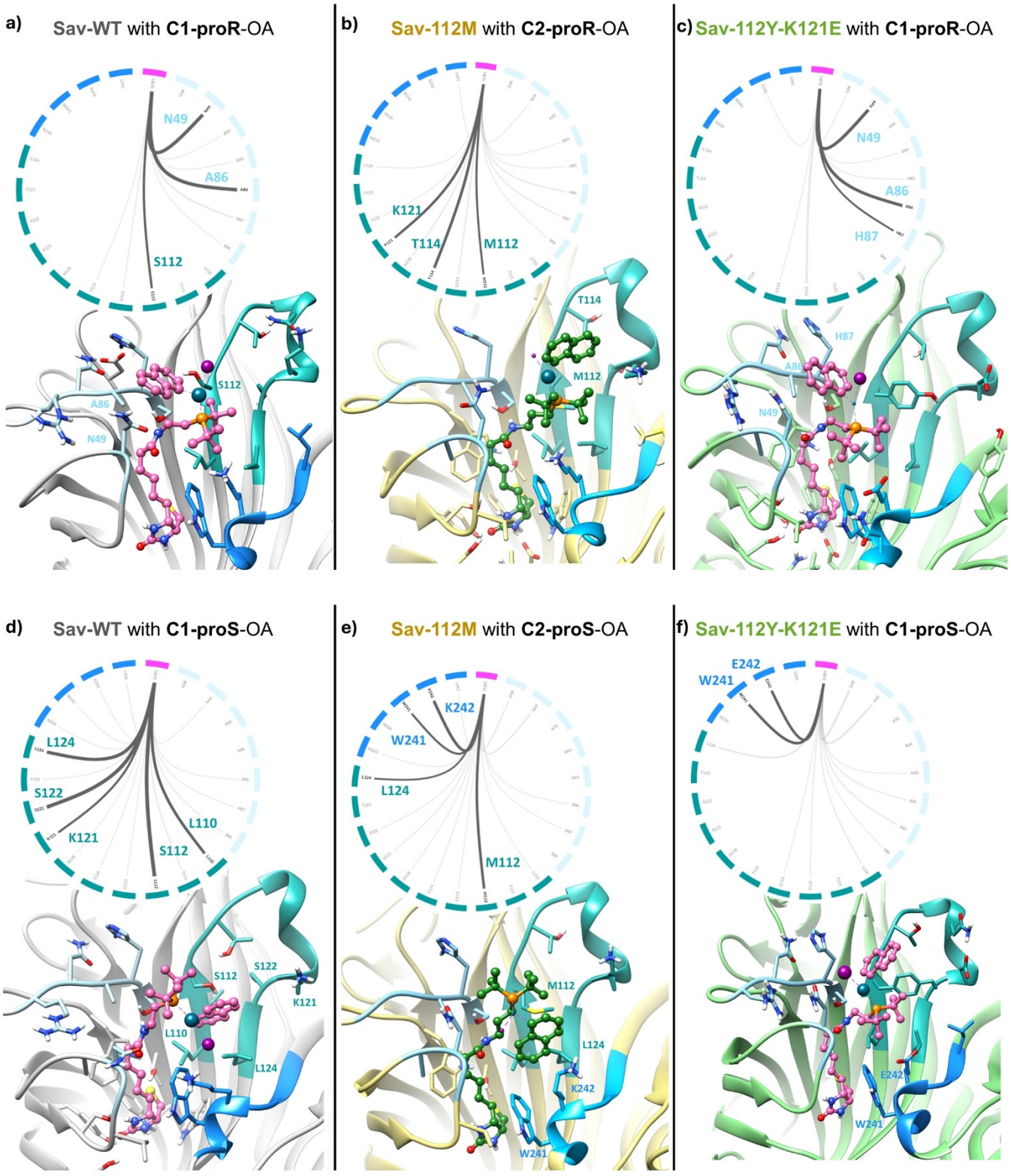

Figure 9. Results of MD simulations of all systems for pro-*R* and pro-*S* OA intermediates. Structure of OA cluster with less clashes and interaction map between intermediate OA and Sav regions.

substrate is only possible in the *biotin-up* conformation as the clashes are low (6.7), but this conformation is only observed in 16% of simulation. In the predominant *biotin-down* conformation there are too many clashes with all surrounding residues (28.6). Experimentally, this system affords 90% ee *R*, which is explained by these simulations in which only in the 16% of the simulations the substrate would be able to enter and obtain the *S* form. For the rest of the simulation of the pro-*S* the second substrate would not be able to enter and afford the *S* product due to the high clashes. It can clearly be stated that the mutation of Tyr112 and Glu121 do not favor OA in the *biotin-up* conformation, which is the one that is favored in the pro-*S*-OA.

MD Simulations with RE-TS

MD simulations of the three systems with **RE-TS** in pro-*R* and pro*S* conformations were performed to assess the stability of final TS in protein environment. The cluster from previous MD simulations with less clashes is used as input and the second substrate is incorporated in the disposition of the **RE-TS**. MD simulations with Sav-S112M show that this system favors the *biotin-up* conformation. During most of the simulation of the pro-*R*, it remains in the *biotin-down* disposition interacting with region A, however, towards the end it acquires the *biotin-up* conformation and interacts mainly with Lys121-242. This indicates that the longer cofactor and Met allows rotating and acquiring the other conformation. In the case of pro-*S*-TS the simulation already starts from *biotin-up* conformation and is also interacting with Lys121-242. In the WT and Sav-S112Y-K12E, both TS, pro-*R* and pro-*S* remain in the same conformation at which the MD simulation starts from, *biotin-down* for pro-*R* and *biotin-up* from pro-*S*. In both cases, the TS moves from region B towards region A to interact manly with Asn47. In pro-*R* from Sav-S112Y-K12E interacts with Tyr112, stabilizing the TS, while in the case of WT Ser does not interact. In the pro-*S* form from WT interaction with Lys242 is maintained during all simulations stabilizing the TS, whereas in the double mutant there is no interaction with E242. These differences in interactions may be related to the favor of *R* in double mutant, as pro-*R* is more stabilized by Tyr and pro-*S* in the WT.

Conclusions

We have studied, by means of an integrative computational approach involving DFT calculations, molecular dockings and MD simulations, the synthesis of enantioenriched binaphthyls catalyzed by an artificial Suzukiase assembled by Ward et al. by incorporating an electron-rich phosphino-palladium moiety (Pd(P(*t*-Bu)$_2$) within a protein (Sav),[17] using biotin-streptavidin technology. Two main features of this system have been analyzed: the influence of the length of the spacer between the biotin anchor and the Pd(P(*t*-Bu)$_2$ on the biaryl enantiomer obtained and the effect of mutations on the reaction outcome. First, the DFT study of the reaction mechanism of SMC biaryl formation in water allows location of all intermediates and transition states along the reaction course and to build up with them a complete Gibbs energy profile for the reaction. Despite the reductive elimination step is the rate-determining step, the oxidative addition and transmetalation steps appear to be irreversible, preventing equilibration of all the intermediates formed to start the reductive elimination step, as already found in a computational investigation of Pd-catalyzed Suzuki-Miyaura cross-coupling synthesis of tetra-*ortho*-substituted biaryls employing P-chiral phosphine ligands.[13] This finding implies that all the three steps contribute to the chiral enantioselection. In this way, one pro-*R* and one pro-*S* intermediate are found as a product of the oxidative addition step.

Docking calculations, followed by molecular dynamics simulations of the precatalytic cofactors, in which palladium is bonded to a chloride and an cinnamyl ligand, with both the short (ethyl, **C1**) and long (propyl, **C2**) cofactors have disclosed that the cofactors can acquire two very different conformations in the protein system, that we have named as *biotin-up* and *biotin-down*. The dihedral angle between atoms P and Pd of the cofactor and alpha carbons from residues 99 and 100 can be used to assess *biotin-up* and *biotin-down* conformations and monitoring its changes along MD simulations.

In principle, the cofactor with the shorter linker **C1** prefers the *biotin-down* conformation whereas that with the longer linker **C2** would prefer the *biotin-up* one. However, these preferences are affected by mutations, which determine if the two conformations can be exchanged of they are kept along the simulation.

The *biotin-up* and *biotin-down* conformations are also found in the oxidative addition intermediates. Molecular Dynamics simulation of these oxidative addition intermediates shows that the pro-*R* OA intermediate tends to preferably acquire the *biotin-down* conformation, whereas the *biotin-up* conformation is favored for the pro-*S* OA intermediate. Moreover, introducing into the MD simulations the structure of the transition state of the reductive elimination reveals that the entrance of the second substrate is more probable for the pro-*R* OA intermediate in the *biotin-down* conformation and for the pro-*S* OA intermediate in the *biotin-up* conformation. However, these tendencies are influenced by the mutations introduced in the system and the length of the cofactors.

Overall, the findings of this study unravel that the enantiomeric differences found experimentally can be rationalized by the disposition of the first intermediate, coming from the oxidative addition step, and the entrance of the second substrate. DFT calculations reveal the overall Suzuki-Miyaura mechanism and indicate that the oxidative addition is the first layer for the enantiodiscrimination and the reductive elimination is the rate determining step. MD simulations of the oxidative addition step with both pro-*R* and pro-*S* products shed light on how their dispositions determine the entrance of the second product and its regioselectivity. From this work it can be concluded that the combination of DFT calculations, molecular dockings and MD simulations can be used to rationalize artificial metalloenzymes. Furthermore, it highlights that standard protocols for the design of ArMs have to be adapted to the catalytic reaction in question to understand the

whole concept. The insight at a molecular level on the action mechanism of Ward's artificial Suzukiase has also showcased the difficulties facing to control the enantioselection when engineering ArM to catalyze enantioselective Suzuki-Miyaura couplings. There is still a lot of room for improvement, and we hope that computational simulations as those collected in this work can contribute to that.

Supporting Information

Supporting information available: Schemes of all the steps of the reaction mechanism, 3-D views, absolute energies and cartesian coordinates of DFT optimized structures, MD simulations of precatalytic cofactors and docking and MD simulations with OA intermediates.

Acknowledgements

We thank the Spanish Ministerio de Ciencia e Innovación for Grant PID2020-116861GB-I00. The allocation of computer time at CSUC is also acknowledged. L T.-S. thanks the Spanish Ministerio de Ciencia, Innovación y Universidades (grant FPU18/05895) for the financial support.

Conflict of Interests

The authors declare no conflict of interest.

Data Availability Statement

The data that support the findings of this study are available from the corresponding author upon request.

Keywords: Artificial metalloenzyme · Asymmetric Suzuki-Miyaura coupling · Biaryl · Integrative computational approach · Molecular modeling

[1] M. J. Buskes, M.-J. Blanco, *Molecules* **2020**, *25*, 3493.
[2] T. K. Koshvandi, M. M. Heravi, T. Momeni, *Appl. Organomet. Chem.* **2018**, *32*, e4210.
[3] a) N. Miyaura, A. Suzuki, *Chem. Rev.* **1995**, *95*, 2457–2483; b) A. Suzuki, *Angew. Chem. Int. Edit* **2011**, *50*, 6722–6737.
[4] M. C. D'Alterio, È. Casals-Cruañas, N. V. Tzouras, G. Talarico, S. P. Nolan, A. Poater, *Chem. Eur. J.* **2021**, *27*, 13481–13493.
[5] a) C. Joshi, J. M. Macharia, J. A. Izzo, V. Wambua, S. Kim, J. S. Hirschi, M. J. Vetticatt, *ACS Catal.* **2022**, *12*, 2959–2966; b) S. J. Firsan, V. Sivakumar, T. J. Colacot, *Chem. Rev.* **2022**, *122*, 16983–17027.
[6] M. García-Melchor, A. A. C. Braga, A. Lledós, G. Ujaque, F. Maseras, *Acc. Chem. Res.* **2013**, *46*, 2626–2634.
[7] G. Hedouin, S. Hazra, F. Gallou, S. Handa, *ACS Catal.* **2022**, *12*, 4918–4937.
[8] J. K. Cheng, S.-H. Xiang, S. Li, L. Ye, B. Tan, *Chem. Rev.* **2021**, *121*, 4805–4902.
[9] a) A. N. Cammidge, K. V. L. Crépy, *Chem. Commun.* **2000**, *18*, 1723–1724; b) J. Yin, S. L. Buchwald, *J. Am. Chem. Soc.* **2000**, *122*, 12051–12052; c) A. Bermejo, A. Ros, R. Fernández, J. M. Lassaletta, *J. Am. Chem. Soc.* **2008**, *130*, 15798–15799; d) R. Pearce-Higgins, L. N. Hogenhout, P. J. Docherty, D. M. Whalley, P. Chuentragool, N. Lee, N. Y. S. Lam, T. M. McGuire, D. Valette, R. J. Phipps, *J. Am. Chem. Soc.* **2022**, *144*, 15026–15032.
[10] a) S. E. Denmark, W.-T. T. Chang, K. N. Houk, P. Liu, *J. Org. Chem.* **2015**, *80*, 313–366;b) R. Jasinski, O. M. Demchuck, D. Babyuk, *J. Chem.* **2017**, *2017*, 3617527.
[11] a) O. Baudoin, *Eur. J. Org. Chem.* **2005**, *2005*, 4223–4229; b) D. Zhang, Q. Wang, *Coord. Chem. Rev.* **2015**, *286*, 1–16.
[12] C. Li, D. Chen, W. Tang, *Synlett* **2016**, *27*, 2183–2200.
[13] N. D. Patel, J. D. Sieber, S. Tcyrulnikov, B. J. Simmons, D. Rivalti, K. Duvvuri, Y. Zhang, D. A. Gao, K. R. Fandrick, N. Haddad, K. S. Lao, H. P. R. Mangunuru, S. Biswas, B. Qu, N. Grinberg, S. Pennino, H. Lee, J. J. Song, B. F. Gupton, N. K. Garg, M. C. Kozlowski, C. H. Senanayake, *ACS Catal.* **2018**, *8*, 10190–10209.
[14] a) O. F. B. Watts, J. Berreur, B. S. L. Collins, J. Clayden, *Acc. Chem. Res.* **2022**, *55*, 3362–3375; b) L. E. Zetzsche, J. A. Yazarians, S. Chakrabarty, M. E. Hinze, L. A. M. Murray, A. L. Lukowski, L. A. Joyce, A. R. H. Narayan, *Nature* **2022**, *603*, 79–85.
[15] F. Schwizer, Y. Okamoto, T. Heinisch, Y. Gu, M. M. Pellizzoni, V. Lebrun, R. Reuter, V. Köhler, J. C. Lewis, T. R. Ward, *Chem. Rev.* **2018**, *118*, 142–231.
[16] T. Heinisch, T. R. Ward, *Acc. Chem. Res.* **2016**, *49*, 1711–1721.
[17] A. Chatterjee, H. Mallin, J. Klehr, J. Vallapurackal, A. D. Finke, L. Vera, M. Marsh, T. R. Ward, *Chem. Sci.* **2016**, *7*, 673–677.
[18] a) V. Muñoz Robles, E. Ortega-Carrasco, L. Alonso-Cotchico, J. Rodriguez-Guerra, A. Lledós, J.-D. Maréchal, *ACS Catal.* **2015**, *5*, 2469–2480; b) L. Alonso-Cotchico, J. Rodríguez-Guerra, A. Lledós, J.-D. Maréchal, *Acc. Chem. Res.* **2020**, *53*, 896–905.
[19] a) V. Muñoz Robles, P. Vidossich, A. Lledós, T. R. Ward, J.-D. Maréchal, *ACS Catal.* **2014**, *4*, 833–842; b) L. Alonso-Cotchico, G. Sciortino, P. Vidossich, J. Rodríguez-Guerra Pedregal, I. Drienovská, G. Roelfes, A. Lledós, J.-D. Maréchal, *ACS Catal.* **2019**, *9*, 4616–4626; c) F. Christoffel, N. V. Igareta, M. M. Pellizzoni, L. Tiessler-Sala, B. Lozhkin, D. C. Spiess, A. Lledós, J.-D. Maréchal, R. L. Peterson, T. R. Ward *Nat. Catal.* **2021**, *4*, 643–653; d) J.-E. Sánchez-Aparicio, G. Sciortino, E. Mates-Torres, A. Lledós, J.-D. Maréchal, *Faraday Discuss.* **2022**, *234*, 349–366.
[20] Gaussian 16, Revision C.01, M. J. Frisch, G. W. Trucks, H. B. Schlegel, G. E. Scuseria, M. A. Robb, J. R. Cheeseman, G. Scalmani, V. Barone, G. A. Petersson, H. Nakatsuji, X. Li, M. Caricato, A. V. Marenich, J. Bloino, B. G. Janesko, R. Gomperts, B. Mennucci, H. P. Hratchian, J. V. Ortiz, A. F. Izmaylov, J. L. Sonnenberg, D. Williams-Young, F. Ding, F. Lipparini, F. Egidi, J. Goings, B. Peng, A. Petrone, T. Henderson, D. Ranasinghe, V. G. Zakrzewski, J. Gao, N. Rega, G. Zheng, W. Liang, M. Hada, M. Ehara, K. Toyota, R. Fukuda, J. Hasegawa, M. Ishida, T. Nakajima, Y. Honda, O. Kitao, H. Nakai, T. Vreven, K. Throssell, J. A. Montgomery Jr, J. E. Peralta, F. Ogliaro, M. J. Bearpark, J. J. Heyd, E. N. Brothers, K. N. Kudin, V. N. Staroverov, T. A. Keith, R. Kobayashi, J. Normand, K. Raghavachari, A. P. Rendell, J. C. Burant, S. S. Iyengar, J. Tomasi, M. Cossi, J. M. Millam, M. Klene, C. Adamo, R. Cammi, J. W. Ochterski, R. L. Martin, K. Morokuma, O. Farkas, J. B. Foresman, D. J. Fox, Gaussian, Inc., Wallingford CT, **2016**.
[21] a) C. Lee, W. Yang, R. G. Parr, *Phys. Rev. B* **1988**, *37*, 785–789; b) B. Miehlich, A. Savin, H. Stoll, H. Preuss, *Chem. Phys. Lett.* **1989**, *157*, 200–206; c) A. D. Becke, *J. Chem. Phys.* **1993**, *98*, 5648–5652.
[22] S. Grimme, J. Antony, S. Ehrlich, H. Krieg, *J. Chem. Phys.* **2010**, *132*, 154104.
[23] S. A. V. Marenich, C. J. Cramer, D. G. Truhlar, *J. Phys. Chem. B* **2009**, *113*, 6378–6396.
[24] D. Andrae, U. Haeussermann, M. Dolg, H. Stoll, H. Preuss, *Theor. Chim. Acta* **1990**, *77*, 123–141.
[25] A. W. Ehlers, M. Bohme, S. Dapprich, A. Gobbi, A. Hollwarth, V. Jonas, K. F. Kohler, R. Stegmann, A. Veldkamp, G. Frenking, *Chem. Phys. Lett.* **1993**, *208*, 111–114.
[26] a) W. J. Hehre, R. Ditchfield, J. A. Pople, *J. Chem. Phys.* **1972**, *56*, 2257–2261; b) M. M. Francl, W. J. Pietro, W. J. Hehre, J. S. Binkley, M. S. Gordon, D. J. DeFrees, J. A. Pople, *J. Chem. Phys.* **1982**, *77*, 3654–3665.
[27] F. Weigend, R. Ahlrichs, *Phys. Chem.* **2005**, *7*, 3297–3305.
[28] G. Jones, P. Willett, R. C. Glen, A. R. Leach, R. Taylor *J. Mol. Biol.* **2002**, *267*, 727–748.
[29] Amber 2020, D. A. Case, K. Belfon, I. Y. Ben-Shalom, S. R. Brozell, D. S. Cerutti, T. E. Cheatham III, V. W. D. Cruzeiro, T. A. Darden, R. E. Duke, G. Giambasu, M. K. Gilson, H. Gohlke, A. W. Goetz, R. Harris, S. Izadi, S. A. Izmailov, K. Kasavajhala, A. Kovalenko, R. Krasny, T. Kurtzman, T. S. Lee, S. LeGrand, P. Li, C. Lin, J. Liu, T. Luchko, R. Luo, V. Man, K. M. Merz, Y. Miao, O. Mikhailovskii, G. Monard, H. Nguyen, A. Onufriev, F. Pan, S. Pantano, R. Qi, D. R. Roe, A. Roitberg, C. Sagui, S. Schott-Verdugo, J. Shen, C. L. Simmerling, N. R. Skrynnikov, J. Smith, J. Swails, R. C. Walker,

J. Wang, L. Wilson, R. M. Wolf, X. Wu, Y. Xiong, Y. Xue, D. M. York, P. A. Kollman, AMBER **2020**, University of California, San Francisco, **2020**.
[30] J. A. Maier, C. Martinez, K. Kasavajhala, L. Wickstrom, K. E. Hauser, C. Simmerling, *J. Chem. Theor. Comput.* **2015**, *11*, 3696–3713.
[31] J. Wang, R. M. Wolf, J. W. Caldwell, P. A. Kollman, D. A. Case, *J. Comput. Chem.* **2004**, *25*, 1157–1174.
[32] W. L. Jorgensen, J. Chandrasekhar, J. D. Madura, R. W. Impey, M. L. Klein, *J. Chem. Phys.* **1983**, *79*, 926–935.
[33] P. Li, K. M. Merz, *J. Chem. Inform. Model.* **2016**, *56*, 599–604.
[34] C. I. Bayly, P. Cieplak, W. D. Cornell, P. A. Kollman, *J. Phys. Chem.* **1993**, *97*, 10269–10280.
[35] J. M. Seminario, *Int. J. Quantum Chem.* **1996**, *60*, 1271–1277.
[36] a) A. Brünger, C. L. Brooks, M. Karplus, *Chem. Phys. Lett.* **1984**, *105*, 495–500; b) T. Schneider, E. Stoll, *Phys. Rev.* B **1978**, *17*, 1302–1322.
[37] U. Essmann, L. Perera, M. L. Berkowitz, T. Darden, H. Lee, L. G. Pedersen, *J. Chem. Phys.* **1995**, *103*, 8577–8593.
[38] J. P. Ryckaert, G. Ciccotti, H. J. Berendsen, *J. Comput. Phys.* **1977**, *23*, 327–341.
[39] E. F. Pettersen, T. D. Goddard, C. C. Huang, G. S. Couch, D. M. Greenblatt, E. C. Meng, T. E. Ferrin, *J. Comput. Chem.* **2004**, *25*, 1605–1612.
[40] a) D. J. Tantillo, J. Chen, K. N. Houk, *Curr. Opin. Chem. Biol.* **1998**, *2*, 743–750; b) G. Kiss, N. Çelebi-Ölçüm, R. Moretti, D. Baker, K. N. Houk, *Angew. Chem. Int. Ed.* **2013**, *52*, 5700–5725; c) J. Rodríguez-Guerra, L. Alonso-Cotchico, G. Sciortino, A. Lledós, J.-D. Maréchal in *Artificial Metalloenzymes and MetalloDNAzymes in Catalysis: From Design to Applications* (Eds.: M. Diéguez, J.-E. Bäckvall, O. Pàmies); Wiley-VCH Verlag GmbH &Co.: Weinheiem, **2018**; pp 99–136.
[41] a) Y. Uozumi, Y. Matsuura, T. Arakawa, Y. M. A. Yamada, *Angew. Chem. Int. Edit.* **2009**, *48*, 2708–2710; b) L. Benhamou, C. Besnard, E. P. Kündig, *Organometallics* **2014**, *33*, 260–266.

Manuscript received: March 22, 2024
Accepted manuscript online: May 16, 2024
Version of record online: ■■, ■■

RESEARCH ARTICLE

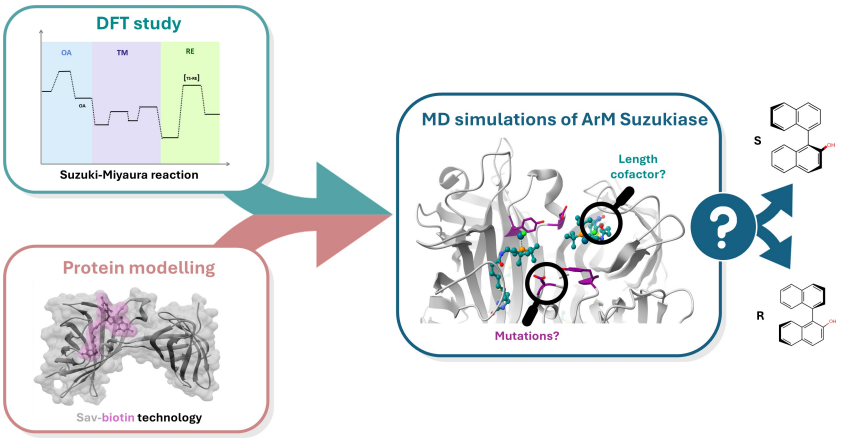

L. Tiessler-Sala, J.-D. Maréchal, A. Lledós**

1 – 14

Rationalization of a Streptavidin Based Enantioselective Artificial Suzukiase: An Integrative Computational Approach

A computational modeling approach is applied to rationalize the impact of streptavidin mutations and length of the biotion cofactor on the enantioselective Suzuki-Miyaura synthesis of binaphthyls by means of an Artificial Metalloenzyme built employing the streptavidin-biotin technology. The integrative computational approach includes DFT calculations, protein-ligand dockings and molecular dynamics simulations.